A novel variant in MFN2 linked to a lethal disorder of neonatal onset

Authors: Mashiat Zaman[1], Julien L Marcadier[2], Amanda V Tyndall[3], Brenda McInnes[2], A Micheil Innes[4], Francois P Bernier[4], Timothy E. Shutt[5]

[1]Department of Biochemistry & Molecular Biology, Cumming School of Medicine, Hotchkiss Brain Institute, Alberta Children's Hospital Research Institute, University of Calgary

[2]Department of Medical Genetics, Cumming School of Medicine, University of Calgary

[3]Department of Medical Genetics, Cumming School of Medicine, Alberta Children's Hospital Research Institute, Hotchkiss Brain Institute, University of Calgary

[4]Departments of Medical Genetics and Pediatrics, Cumming School of Medicine, Alberta Children's Hospital Research Institute, University of Calgary

[5]Departments of Medical Genetics and Biochemistry & Molecular Biology, Cumming School of Medicine, Hotchkiss Brain Institute, Snyder Institute for Chronic Diseases, Alberta Children's Hospital Research Institute, University of Calgary

Abstract:

Pathogenic variants in the mitochondrial fusion protein Mitofusin2 typically cause axonal Charcot-Marie-Tooth disease type 2A (CMT2A), a progressively degenerative peripheral neuropathy. Here, we present two siblings with a lethal disorder of neonatal onset who carried a novel homozygous MFN2 variant R334K. Given the severe clinical presentation, which is atypical of MFN2 variants, further functional investigations were warranted to confirm the pathogenicity of the R334K variant, which was deemed to be likely pathogenic. Characterization of patient fibroblasts showed severe disruptions all MFN2-related functions that were assayed, including reduced mitochondrial respiration, altered mito-ER contacts, decreased mtDNA copy number and size, as well as increased abundance of cellular lipid droplets. We also observed reduced Complex I activity, which is noted in cells lacking MFN2, but is not standard for pathogenic MFN2 variants that cause CMT2A. These functional deficits, combined with the fact that loss of MFN2 is lethal in model organisms (e.g. mice/fruit-flies), support the notion that the MFN2 R334K is a loss of function variant that is responsible for patient phenotype. Thus, we present a novel pathogenic MFN2 variant causing severe fatal neonatal disease.

Synopsis Statement:

This work identifies a novel homozygous MFN2 variant, R334K, in two individuals with neonatal onset of fatal disease.

33 **Introduction:**

34 Pathogenic variants in *MFN2* cause the hereditary motor sensory neuropathy Charcot-Marie-
35 Tooth disease 2a (CMT2a), which is characterized by progressively worsening pain, numbness and
36 weakness in the distal regions of the body. CMT2a is generally seen as an early-onset disease, with
37 symptoms typically appearing around the age of 10. While CMT2a is most often autosomal dominant
38 (CMT2A2A), there are cases of homozygous or compound heterozygous recessive inheritance
39 (CMT2A2B) [1,2]. *MFN2* encodes the integral outer mitochondrial membrane (OMM) protein Mitofusin2
40 (MFN2), initially characterized for a role in mitochondrial fusion [3]. The protein consists of distinct
41 domains, with an N-terminal GTPase domain, followed by two coiled-coiled heptad repeat (HR) domains
42 separated by a transmembrane domain.

43 The clinical presentation of CMT2a can vary widely, where some MFN2 variants are associated
44 with additional patient pathology [4–6]. While there is evidence of specific MFN2 variants leading to severe
45 and early pathology, neonatal lethality is exceedingly rare and there is one report of antenatal onset [7–10].
46 Though the reasons for this heterogeneity are unknown, it is notable that MFN2 has several other
47 functions, including mediating mito-ER contacts (MERCs) [11], facilitating mito-lipid droplet contacts [12],
48 participating in mitochondrial transport [13] and being a key regulator of mitophagy [14]. These MFN2
49 functions also influence downstream processes such as mtDNA regulation [15], cellular Ca^{2+} signalling [16]
50 and mitochondrial bioenergetics [17]. The impact of different MFN2 variants on the various functions of
51 MFN2 is largely unknown [17]. Surprisingly, for the few variants that have been studied fusion is not
52 always impacted, suggesting that other MFN2 functions are also important in the context of pathology.

53 In this work, we describe two siblings who presented with areflexia, hypotonia and restricted
54 movement upon birth, and who harbored a novel homozygous variant of unknown significance in MFN2,
55 c.1001G>A, p.(Arg334Lys), which was deemed worthy of further investigation. We report detailed
56 patient pathology and provide a comprehensive fibroblast characterization of mitochondrial functions
57 associated with MFN2 that may contribute to the clinical outcomes.

58 **Methods**

59 **Genomic analysis**

60 The proband was enrolled into a research study titled Rapid Access for Pediatric Diagnoses
61 Kidomics (RAPiD) at the Alberta Children's Hospital. Formal written consent was provided by the
62 family (mother, father, and proband) for both the RAPiD research exome (study approved by
63 the University of Calgary Conjoint Health Research Ethics Board) sequencing and the clinical
64 whole exome sequencing. DNA was extracted from whole blood samples, and trio exome
65 library preparation was conducted using the xGen Exome Research Panel v1.0 capture kit
66 (Integrated DNA Technologies, Inc., Coralville, IA, USA). Paired-end sequencing was performed
67 on a NextSeq 550 (Illumina, San Diego, CA, USA) in which data was automatically uploaded into
68 BaseSpace Sequencing Hub where alignment, variant calling, and variant interpretation was
69 completed.

70 **Sequence alignment**

71 Amino acid sequence alignment was performed on T-COFFEE multiple sequence alignment tool
72 [18]. Protein sequences were collected from the UniProt database [19]. Human MFN2: O95140-1; Human
73 MFN1: Q8IWA4; Mouse MFN2: Q80U63; Fish MFN2: A8WIN6; Fly MFN2: Q7YU24; Worm MFN2:
74 Q23424; FXRD1: Q96CU9; FXRD1 [2]: Q96CU9-2 ; FXRD1 [3]: Q96CU9-3; Mouse FXRD1: Q3TQB2; Fish
75 FXRD1: A0A0R4IHD6; Fly FXRD1: Q9VJ10; Worm FXRD1: A0A0V1BI76 .

76 **Cell culture**

77 Skin fibroblasts were cultured in Minimum Essential Media (Gibco™, 11095098), supplemented
78 with 10% Fetal Bovine Serum (FBS) and 10mM Sodium Pyruvate. The cells were maintained at 37°C and
79 5% CO_2.

80 **Respiration studies**

81 Cellular oxygen consumption rates were measured using the Seahorse XFe24 Extracellular Flux
82 Analyzer (Agilent Technologies) as previously described [20]. In summary, cells were seeded in the
83 manufacturer provided microplate at 70,000 cells/well and incubated for 24 hours at 37°C and 5% CO_2.
84 Subsequently, the growth media was replaced, and cells equilibrated in assay media supplemented with
85 d-Glucose (25 mM), sodium pyruvate (2 mM) and l-Glutamine (4 mM). Oxygen consumption rates were

86 calculated following administration of the following compounds: Oligomycin (1 µg/mL) (Enzo Life
87 Sciences, BML-CM111), Carbonyl Cyanide 4-(trifluoromethoxy) Phenylhydrazone (FCCP, 1 µM) (Enzo life
88 Sciences, BML-CM120) and Antimycin A (1 µM) (Sigma Aldrich, A8674). The data from the Seahorse
89 analyzer was normalized to protein content data for each well measured by BCA assay (Thermo Fisher
90 Scientific, 23225).

91 **Immunofluorescence and Microscopy**

92 Control and patient fibroblasts were seeded on coverslips (Fisherbrand, 12-545-81) at a density
93 of 20,000 cells and incubated for 24 hours at at 37°C and 5% CO_2. Cells were fixed with 4%
94 paraformaldehyde at 37°C for 20 minutes, permeabilized using 0.1% Triton® X-100 (MP Biomedicals,
95 9002-93-1) and blocked with 10% FBS. The mitochondrial network was stained with anti-TOMM20
96 (Sigma-Aldrich, HPA011562/Santa Cruz Biotechnology, F-10 sc-17764) primary antibodies and visualized
97 using goat anti-rabbit secondary conjugated with Alexa Fluor 488 (ThermoFisher, A-11034) or goat anti-
98 mouse conjugated Alexa Fluor (ThermoFisher, A-31571). Mitochondrial nucleoids were visualized using
99 anti-dsDNA antibody (Developmental Studies Hybridoma Bank, AB_10805293) and goat anti-mouse
100 secondary conjugated with Alexa fluor 568 (ThermoFisher, A-11004), following permeabilization with
101 0.2% Triton® X-100**.** Lipid droplets were tagged using anti-PLIN1 antibody (Cell Signalling Technology,
102 9349S). Confocal imaging was performed using Olympus spinning disc confocal system (Olympus SD
103 OSR) (UAPON 100XOTIRF/1.49 oil objective). STED imaging was performed using Leica TauSTED
104 microscope. The mitochondrial network was analyzed using the MiNA plugin on FIJI [21]**.**

105 **Proximity Ligation Assay:**

106 The proximity ligation assay was performed as mentioned in [6]. All immunostaining steps,
107 including fixation, blocking and permeabilizing were the same as mentioned above. The Duolink® In Situ
108 Proximity Ligation Assay (Millipore Sigma) was used for this. The aforementioned TOMM20 was used to
109 label the mitochondria and the ER was labelled using anti-Calnexin (mouse monoclonal, EMD Millipore:
110 MAB3126 (RRID:AB_2069152). Images were analyzed using confocal microscopy (as described above)
111 and PLA puncta were analyzed using the 'analyze particles' tool on FIJI.

112 **Western Blot Analysis**

113 Cells at the same confluency were collected and RIPA buffer (Thermo Scientific™, 89900)
114 complimented with protease inhibitors was used to lyse and collect the protein extracts. Following
115 quantification of protein concentrations, 50 µg of total protein from control and patient fibroblasts were

116 loaded on an SDS-PAGE gel. Subsequently, PVDF membranes were used for overnight transfer of the
117 blots. The blots were probed with the following antibodies: anti-MFN2 (Abnova, H00009927-M03;
118 1:1000), anti-MFN1 (Cell Signaling Technology, D6E2S; 1:1000), anti-OPA1 (BD Transduction
119 Laboratories, 612607; 1:1000), anti-Actin (Sigma, A5316; 1:1000) and cocktail anti-OXPHOS Complex
120 antibody (AbCam, ab110411). Complimentary horseradish peroxidase conjugated antibodies were used:
121 goat anti rabbit IgG, HRP linked Antibody (Cell Signaling Technology, 7074S) or goat anti-mouse IgG-HRP
122 (Santa Cruz Biotechnology, sc-2055). Blots were treated with the SuperSignal™ West Femto Maximum
123 Sensitivity Substrate (Thermo Scientific™, 34095), and luminescence visualized with an Amersham
124 Imager AI600.

125 **mtDNA Copy Number and mtDNA Deletions Analysis**

126 Total DNA was extracted and purified from control and patient fibroblasts seeded at 30,000 cells
127 using the PureLink Genomic DNA Mini Kit (Thermo Fisher Scientific, K182001) using the given protocol.
128 Relative mtDNA copy number was analysed using QuantStudio 6 Flex Real-Time PCR system (Thermo
129 Fisher Scientific). The mtDNA and nuclear encoded housekeeping gene 18S were amplified using the
130 primers and reaction conditions described in [22]. Long range PCR reactions were performed to examine
131 mtDNA deletions. The following primers were used for amplification of the mtDNA: 1482–1516 F:
132 ACCGCCCGTCACCCTCCTCAAGTATACTTCAAAGG; 1180–1146 R:
133 ACCGCCAGGTCCTTTGAGTTTTAAGCTGTGGCTCG. The Takara LA Taq Polymerase (Takara Bio, RR002M)
134 was used with 250ng total cellular DNA. PCR cycling conditions were 94°C for 1 min; 98°C for 10 s and
135 68°C for 11 min (step 2 and 3- 35 cycles); and a final extension cycle at 72°C for 10 min, using an
136 Eppendorf® 5331 MasterCycler Gradient Thermal Cycler. PCR products were visualized by
137 electrophoresis on a 0·6% agarose gel, run for approximately 18 h at 20 V.

138 **Complex-I Activity Assay**

139 The mitochondrial complex-I activity assay was performed using the Complex I Enzyme Activity
140 Dipstick Assay Kit (AbCam, ab109720) according to manufacturer instructions. Briefly, 50,000 cells were
141 seeded and collected the following day. 10x Extraction buffer from the kit was added to the cell pellet
142 and subsequently spun at 18,000 x g. Supernatants were collected and following homogenization,
143 control and patient samples were plated in the plate provided. Subsequently, the dipstick from the plate
144 was added and incubated for 45 minutes. Following washing procedures, the dipsticks were imaged with
145 Amersham Imager AI600.

146 **Statistical Analyses**

147 All statistical analyses were performed using GraphPad Prism 9.

148

149 **Results:**

150 **Case description:**

151 Proband (P1)

152 The male proband was born by C-section for preterm labor, breech presentation and fetal heart
153 rate abnormalities to a 21-25-year-old G3, P0 mother. The pregnancy was remarkable only for a mild
154 COVID infection in the first trimester with three antenatal ultrasounds reported as completely normal.
155 Decreased fetal movements were noted in the last 4 to 8 weeks of the pregnancy. His birthweight was in
156 the 10th percentile, length was in the 50th percentile, and head circumference was in the 50th
157 percentile. APGARs were 1,3,3,6 at 1, 5,10 and 15 minutes respectively. He remained flat with no
158 respiratory effort and was intubated at 6 minutes of life. He remained ventilator dependent and
159 eventually died in the pediatric intensive care unit at 2-6 weeks of age. On examination he was noted to
160 have hypotonia both peripherally and axially with decreased spontaneous movements. He had bilateral
161 flexion contractures at his elbows and knees with limited hip abduction and talipes equinovalgus. He
162 was noted to have a bulbous nasal tip but a complete dysmorphology exam was not feasible.

163 Investigations included normal newborn metabolic screening, normal rapid aneuploidy
164 detection, SNP chromosomal microarray, Prader Willi, DM-1 and SMA. While chromosomal microarray
165 analysis did not reveal any copy number variation to explain the proband's phenotype, the SNP
166 component of the analysis revealed three contiguous regions (greater than 10Mb) of absence of
167 heterozygosity (AOH) within chromosomes 1, 3, and 4. Metabolic investigations revealed normal urine
168 and plasma amino acids and a normal plasma acylcarnitine profile. Urine organic acids were non
169 diagnostic and plasma 3-methylglutaconic acid and 3-methylglutaric acid were also normal. EEG was
170 indicative of moderate diffuse/multifocal cerebral dysfunction with multifocal epileptiform discharges.
171 Brain MRI shortly after birth showed multiple foci of diffusion restriction due to cytotoxic edema
172 involving the deep and periventricular white matter in frontoparietal lobes with corresponding intrinsic
173 T1 hyperintensity. There were no overt signs on imaging or MRS to suggest a metabolic cause. A follow-
174 up brain MRI just prior to death reported interval resolution of the multiple foci of restricted diffusion in

175 the bilateral centrum semiovale ovale/corona radiata, with a few small scattered residual centrum
176 semiovale T1 hyperintense foci without restricted diffusion. As compared to the previous MRI, there was
177 interval development of atrophy of the superior vermis, seen as increased interfoliate distance. Mild
178 atrophy was also seen involving the lateral cerebellar hemispheres. The brain stem structures, especially
179 the midbrain and pons, had reduced volume for patient's age, with prominence of the prepontine
180 cisterns, resulting in prominence of the posterior fossa CSF spaces without mass effect. The remainder
181 of the midline structures appeared normal with no Chiari I deformity and a normal pituitary gland. The
182 corpus callosum was well developed and the remaining brain parenchyma was normal with an age-
183 appropriate myelination pattern. No new areas of restricted diffusion or abnormal signal involving the
184 cerebrum or cerebellum were observed and there was no abnormal susceptibility-related signal loss to
185 suggest blood degradation products. The brain stem structures, especially the midbrain and pons had
186 reduced volume for the patient's age. Additional imaging of the patient's spine showed marked smooth
187 hypoplasia and reduced caliber of the thoracic spinal cord. In addition, the brainstem and thoracic spinal
188 cord reported to be small.

189 A muscle biopsy was performed shortly before death revealing no definite abnormalities but
190 coarse NADH, SDH, and COX histochemistries were observed in addition to mild mitochondrial
191 aggregation in the subarcolemmal spaces with some smaller mitochondria but normal cristae. There
192 were grouped atrophic fibres and occasional hypertrophic fibres.

193 Proband's sibling (P2)

194 The proband's male sibling presented with the same core phenotype of encephalopathy,
195 hypotonia, hyporeflexia, arthrogryposis. The sibling had an unremarkable prenatal history with normal
196 initial anatomy scan. A second prenatal scan revealed breech presentation but otherwise normal with
197 normal fetal movements. A further scan was appropriate for gestational age and showed breech
198 presentation. He was born via C-section due to preterm labor with APGARS 1, 2, and 3 at 1, 5 and 10
199 minutes respectively, with no spontaneous respirations. He was intubated and admitted to NICU. He
200 required continuous mandatory ventilation. Life sustaining measures were withdrawn between day 11-
201 15 and the patient died the same day. An autopsy was declined.

202 On examination at birth, the baby was noted to be hypotonic with contractures and decreased
203 range of motion of elbows, hips and knees with bilateral talipes equinovarus. His birth weight was in the
204 50th percentile, length was in the 90th percentile, and head circumference was in the 50th percentile. He

205 had depressed/absent reflexes. Investigations included a normal newborn metabolic screen, normal
206 lactates, ammonia, and liver enzymes with a mildly elevated CK. An EEG was consistent with
207 encephalopathy. Brain MRI showed cerebellar hypoplasia with query germiolytic cysts. An MRI of the
208 spine was normal.

209 **Genetic workup**:

210 Upon initial research RAPID exome sequencing, trio analysis of P1 and parents, who were
211 distantly consanguineous, detected the homozygous c.1001G>A, p.(Arg334Lys) variant of uncertain
212 significance in the MFN2 gene. Pathogenic variants in MFN2 are associated with autosomal dominant
213 and autosomal recessive Charcot-Marie-Tooth disease, axonal, type 2A. While patients with variants in
214 MFN2 have a heterogeneous clinical presentation with an age of onset ranging from 1-45 years,
215 previously reported individuals with homozygous or compound heterozygous variants presented before
216 the age of 10 years [23,24]. These affected individuals presented with muscle weakness, distal sensory loss,
217 and normal or mildly decreased nerve conduction velocity, while the heterozygous parents were
218 reported to be asymptomatic or had signs of a mild peripheral neuropathy [24]. This variant has not been
219 reported in gnomAD, ClinVar, or the literature. This missense variant resides near the middle of exon 10
220 of 19 and appears to abolish a potential cryptic donor splice site within this exon. The consequence of
221 the loss of this cryptic donor splice site is unknown. A subsequent clinical exome of P1 confirmed the
222 homozygous MFN2 c.1001G>A, p.(Arg334Lys) variant, and also found a novel homozygous missense
223 variant of unknown significance, c.1454T>A, p.(Ile485Asn), in FOXRED1, a gene associated with complex
224 I deficiency [25–28].

225 Sanger sequencing was used to assess the genetic status of P2. Analysis found homozygosity for
226 MFN2 Arg334Lys, but only heterozygosity for FOXRED1 Ile485Asn. The family also had an unaffected
227 sister, for whom no genetic information was obtained.

228 Based on the genetic work-up from P1, we initially considered both MFN2 R334K and FOXRED1
229 I485N variants. Given that the candidate variants in MFN2 and FOXRED1 have not been described or
230 characterized previously, we examined the conservation of the corresponding amino acid changes in the
231 protein. We found that the MFN2 R334 residue is conserved in multiple species, including fruit flies and
232 worms, as well as in the paralogous protein MFN1, arguing that it plays an important role in protein
233 function (Figure 1A). Meanwhile, though the FOXRED1 I485 residue is conserved in vertebrates, it is not
234 conserved in earlier diverging metazoans such as flies or worms (Figure 1B). Upon subsequent

235 sequencing of P2, who was homozygous for MFN2 R334K, but only heterozygous for and FOXRED1
236 I485N, it became evident that MFN2 R334K was most likely the causative variant for the remarkably
237 consistent phenotype in the two brothers.

238 **Characterization of patient fibroblasts harboring MFN2 R334K:**

239 As the candidate pathogenic variant in MFN2 is novel and has not been characterized previously,
240 fibroblasts from a skin biopsy of P1, who harboured homozygous MFN2 R334K and FOXRED1 I485N
241 variants, were obtained for functional analysis. We examined a variety of cellular and mitochondrial
242 phenotypes to see which, if any, might be consistent with MFN2 and/or FOXRED1 dysfunction.
243 Unfortunately, fibroblast cells were not available for P2.

244 **Patient fibroblasts show evidence of mitochondrial dysfunction:**

245 Given the integral role of mitochondria in ATP production, we first assessed oxygen
246 consumption in patient fibroblasts, as this is a key indicator of changes to mitochondrial function.
247 Compared to control cells, we observed marked decreases in both basal and maximal oxygen
248 consumption (Figure 2A), as well as spare respiratory capacity (Fig 2B). These findings are indicative of
249 reduced mitochondrial respiration in patient fibroblasts, consistent with an underlying mitochondrial
250 dysfunction contributing to the patient phenotype.

251 Next, we investigated the canonical function of MFN2 in mitochondrial fusion by visualizing the
252 mitochondrial network after immunofluorescent labeling for the mitochondrial marker TOMM20 (Figure
253 2C). In comparison to the control fibroblasts, which showed elongated and reticular mitochondrial
254 network morphology, patient fibroblasts qualitatively displayed more fragmented mitochondrial
255 networks (Figure 2D). Quantitative analysis of the mitochondrial networks confirmed patient fibroblasts
256 had shorter mitochondria (Figure 2E). Together, these findings are consistent with impaired
257 mitochondrial fusion leading to more fragmented mitochondria.

258 **Changes in mitochondrial nucleoids and mtDNA copy number depletion in patient fibroblasts:**

259 To provide further evidence of impaired mitochondrial fusion, we investigated the distribution
260 and abundance of mtDNA, which can be altered by impairments to mitochondrial fusion, are linked to
261 loss of MFN2 function, and have been observed for some MFN2 variants [17,29,30]. Immunofluorescence
262 imaging of mtDNA nucleoids (Figure 3A) revealed that the patient fibroblasts exhibited approximately
263 half as many nucleoids as control fibroblasts (Figure 3B), and that patient mtDNA nucleoids were smaller

264 (Figure 3C). Consistent with the reduced number of mtDNA nucleoids, we detected a 40% decrease in
265 the mtDNA copy number in the patient fibroblasts via qPCR (Figure 3D). Finally, we also investigated the
266 presence of mtDNA deletions, which are sometimes seen with MFN2 loss of function [17]. However, no
267 mtDNA deletions were detected (Figure 3E).

268 **Altered mito-ER contact sites and lipid droplet accumulation in patient fibroblasts:**

269 We investigated the size and abundance of mito-ER contact sites (MERCs) and lipid droplets, as
270 these phenotypes can be altered in fibroblasts from patient harboring pathogenic MFN2 variants [6,31]. As
271 a proxy for MERCs, we utilized a proximity ligation assay (PLA) that generates a fluorescent signal when
272 mitochondria and ER are within ~40 nm (Figure 4A,4B) [32]. Using confocal microscopy, we observed a
273 decrease in the size and number of MERCs, which was confirmed by quantitative analyses (Figure 4C,D).
274 We examined lipid droplets by immunofluorescence with the lipid droplet surface protein Perilipin 1
275 (Figure 5A). Compared to control fibroblasts, we noted a distinct upregulation in the number (Figure 5B)
276 and size (Figure 5C) of PLIN1 puncta in the R334K patient fibroblasts. These findings of decreased MERCs
277 and increased lipid droplets are consistent with previously reported alterations in fibroblasts from
278 patients with CMT2A harbouring MFN2 variants [12,31].

279 **MFN2 and mitochondrial protein expression:**

280 As our findings were consistent with MFN2 dysfunction, we assessed if expression of MFN2 and
281 other mitochondrial proteins was impacted. While we did not observe changes in MFN2 protein levels
282 from total cell lysate (Figure 6a-b), we did observe a significant (~50%) decrease in expression of the
283 nuclear DNA encoded mitochondrial complex I subunit NDUFB8 (Figure 6A,C). Notably, there was no
284 consistent significant change to the levels of the other OXPHOS proteins investigated here, including
285 mtDNA-encoded MTCO1. The cause for this discrepancy in OxPhos protein expression is unknown, but
286 likely does not reflect the mtDNA depletion, which would be expected to cause a global decrease in
287 OxPhos protein expression as mtDNA encodes essential proteins for all the electron transport chain
288 complexes except for complex II.

289 **Complex I activity:**

290 Given the specific decrease in a Complex I protein, which is not typical of MFN2 dysfunction and
291 likely not explained by mtDNA depletion, we wondered if the identified FOXRED1 missense variant
292 might also have functional consequences that could contribute to the patient phenotype. As pathogenic
293 defects in FOXRED1 are linked to dysfunction in complex I assembly and stability, we also examined

294 Complex I activity. Consistent with the reduced protein expression, and possible complex I instability, we
295 observed an ~50% reduction in Complex I activity in patient fibroblasts (Figure 6D,E).

296

297 **Discussion:**

298 We report two siblings who presented with severe hypotonia, areflexia and limited movement
299 upon birth, who both harboured a novel homozygous single missense variant in MFN2 p.(Arg334Lys).
300 Though CMT2A can be an early-onset disease that can eventually restrict patient movement as the
301 disease progresses, the patients reported here exhibited lack of movement upon birth, indicative of a
302 more severe disease onset. Moreover, both patients succumbed in infancy (<6 weeks). Though areflexia
303 and hypotonia phenotypes are not typical of CMT2A, there are a few previous reports of both these
304 phenotypes in patients harbouring MFN2 variants with severe early onset disease prognosis [23,30,33–36].
305 However, the patients we report here presented with symptoms immediately upon birth, as opposed to
306 the examples in the previous reports, where symptoms presented from 6-12 months. With respect to
307 the early onset of severe phenotypes linked to MFN2 dysfunction, there is a recent report of a patient
308 with severe CNS complications who harboured a homozygous 50 amino acid deletion in MFN2 with
309 antenatal presentation that resulted in pregnancy termination at 31 weeks [10]. In this regard, the fact
310 that loss of MFN2 function leads to embryonic lethality in mice [3] and larval lethality in fruit flies [37], is
311 consistent with a severe loss of MFN2 function due to the R334K variant.

312 In support of the notion that the R334K variant impairs MFN2 functions, we observed changes
313 across all the functions we explored, including mitochondrial network morphology, oxidative
314 phosphorylation, complex I activity, MERCs, mtDNA copy number and nucleoids, as well as cellular lipid
315 droplets. These findings suggest that the novel R334K variant causes severe dysfunction of the MFN2
316 protein. To our knowledge, there are no previously characterized MFN2 CMT2a variants with defects
317 across all these functions [17]. However, this finding likely reflects the fact that few MFN2 variants have
318 been characterized extensively for their impact on MFN2 functions, highlighting our limited
319 understanding of how MNF2 variants impact MFN2 functions. In terms of MFN2 variants associated with
320 more severe cellular phenotypes, it is notable that MFN2 variants that correlate with reduced mtDNA
321 copy number and impaired oxidative phosphorylation are reported in patients that tend to present with
322 earlier-onset and severe clinical outcomes [6,38,39]**.** Collectively, this evidence is consistent with severe

323 MFN2 dysfunction contributing to the very early onset of clinical symptoms in the patients we report
324 here.

325 It is also worth briefly discussing the Complex I deficiency in P1, which is not typical of
326 pathogenic MFN2 variants, especially in light of the additional homozygous FOXRED1 variant in this
327 patient. Notably, complete loss of MFN2 function can lead to a specific deficit in complex I expression
328 and function [40]. Moreover, Complex I dysfunction was also reported with the MFN2 variant harbouring a
329 50 amino acid deletion where the patient also presented immediately upon birth with a severe
330 phenotype [10]. Thus, MFN2 dysfunction alone is sufficient to cause Complex I deficiency.

331 Though FOXRED1 is a molecular chaperone that is important for the assembly of mitochondrial
332 complex I [25,41], several lines of evidence argue against a potential role for the I485N variant contributing
333 to the phenotype of the patients. First, the patient phenotypes do not match. Homozygous or
334 compound heterozygous recessive FOXRED1 variants cause mitochondrial complex I deficiency, nuclear
335 type 19 (MC1DN19), where only a handful of cases have been described [25,26,28,42–45]**.** Clinical phenotypes
336 of MC1DN19 mimic common mitochondrial disorders such as Leigh syndrome and mitochondrial
337 encephalopathy [42,43,46], including lactic acidosis and growth restrictions. In contrast, there was no
338 evidence of lactic acidosis in P1 or P2. Meanwhile, though MC1DN19 patients can have hypotonia [28,42],
339 and can also be diagnosed with restricted movement accompanying Leigh syndrome [25], there are no
340 reports of areflexia in FOXRED1 patients, who typically survive well past infancy [26]. Secondly, the
341 genetics also argue against I485N FOXRED1 variant contributing to pathology, as FOXRED1 is autosomal
342 recessive, while P2 was heterozygous for the I485N FOXRED1 variant. Thus, despite the fact that novel
343 I485N FOXRED1 variant reported here is located at the C-terminus of the protein, similar to other
344 pathogenic FOXRED1 variants described to date, and the fact that FOXRED1 patient fibroblasts also have
345 reduced Complex I activity [28] (with patient myoblasts reported with deficiencies in both Complex I and
346 Complex II [44]), this variant was ruled out as a contributing factor for the phenotype of P1 and P2, who
347 had identical presentations. Of note, it is also possible that the FOXRED variant may have contributed to
348 a milder phenotype that was masked by the more severe MFN2 disorder.

349 Rapid whole exome sequencing (WES) has repeatedly shown that a quicker time to diagnosis
350 guides goals of clinical care, including less failed treatments, and ultimately lowers the financial burden
351 on the health care system [47–49]. While previous reports suggests that between 30-50% of WES cases are
352 solved or partly solved by a known disease-associated gene, additional cases may reveal novel genes of
353 uncertain significance (GUS). This study demonstrates the utility of rapid WES accompanied by

354 functional experiments to assess these GUS and provide a diagnosis. Functional studies also have the
355 potential to discover new treatment options for novel genes. However, as this study demonstrates, this
356 is dependent upon the damaging effects of the variant on the normal function of the gene and/or
357 protein. Regardless, this study demonstrates the value of collaboration between clinical and research
358 colleagues.

359 To summarize our findings, we report severe clinical symptoms upon birth in two siblings
360 homozygous for the novel MFN2 R334K variant, and observed numerous cellular dysfunctions in patient
361 fibroblasts that can be explained by loss of MFN2 function. Thus, we speculate the location of the R334K
362 MFN2 variant is crucial for proper protein function, possibly by altering the nearby GTPase domain of
363 the protein. In summary, we suggest the novel MFN2 R334K variant significantly impairs the MFN2
364 protein and is causative of the severe patient phenotype.

365

366 **Acknowledgements**

367 The authors would like to thank the study participants and their family. We would also like to
368 thank Matthew Lines for his input on the manuscript.

369

370 **Conflict of Interests**

371 The authors declare that they have no conflict of interest.

372

373 **Author contributions**

374 Designed and/or performed and analyzed mitochondrial experiments, MZ and TES; Clinical
375 evaluation of patients and write up, JLM, BM, AMI, FPB; Analyzed exome data AVP; Drafted the
376 manuscript or figures, MZ, AVP, BM, TES. All authors discussed the results and commented on the
377 manuscript.

378

379 **Funding**

380 This work was supported by funds provided by the Canadian Institutes of Health Research (TES)
381 and the Alberta Children's Hospital Research Institute (Owerko Center) (MZ). MZ was supported by a
382 Hotchkiss Brain Institute International Recruitment Scholarship. The funders had no role in study design,
383 data collection and interpretation, or the decision to submit the work for publication.

384 **Figure Legends:**

385 **Figure 1: Importance (conservation) of amino acid variants in MFN2/FXRD1.** Multiple sequence
386 alignment showing (A) MFN2 conservation of arginine-334 and (B) FOXRED1 conservation of isoleucine
387 485. Accession numbers: Human MFN2: O95140-1; Human MFN1: Q8IWA4; Mouse MFN2: Q80U63; Fish
388 MFN2: A8WIN6; Fly MFN2: Q7YU24; Worm MFN2: Q23424 ; FXRD1: Q96CU9; FXRD1 [2]: Q96CU9-2 ;
389 FXRD1 [3]: Q96CU9-3; Mouse FXRD1: Q3TQB2; Fish FXRD1: A0A0R4IHD6; Fly FXRD1: Q9VJ10; Worm
390 FXRD1: A0A0V1BI76 .

391

392 **Figure 2: Mitochondrial dysfunction and network fragmentation in patient fibroblasts.** Oxygen
393 Consumption Rate (OCR) for control and patient fibroblasts, showing the Seahorse Mitochondria Stress
394 Test profile (A) and quantification of spare respiratory capacity (B), using two biological replicates with
395 10 technical replicates each, bar graphs indicate mean +/- SD. (C) Representative super resolution (STED)
396 microscopy immunofluorescence images showing mitochondrial network morphology, stained using
397 anti-TOMM20. (D) Qualitative analysis of mitochondrial branch appearance
398 (fused/intermediate/fragmented) analyzed using two biological replicates with 50 cells for each, bar
399 graphs indicate mean for each category +/- SD. (E) Average mitochondrial branch lengths in control and
400 patient fibroblasts, analyzed from 2 biological replicates with 50 cells for each replicate. Violin plots
401 indicate median and interquartile range. For all graphs, p-values were determined by unpaired t-test (*
402 indicates $p \leq 0.05$, ** $p \leq 0.01$, *** $p \leq 0.001$, ***$p \leq 0.0001$).

403

404 **Figure 3: MtDNA alterations in patient fibroblasts.** (A) Representative confocal microscopy images
405 showing DAPI (nucleus; blue) and mitochondrial nucleoids (anti-dsDNA; red) co-localized with the
406 mitochondrial network (anti-TOMM20; teal) for control (top panels) and patient fibroblasts (bottom
407 panels). Quantitative analyses of average number of mitochondrial nucleoids per cell (B) and average
408 size (C) per cell in control and patient fibroblasts, analyzed from 2 biological replicates with 40 cells for
409 each category; red and blue colors indicate different biological replicates; lines indicate mean +/- SD. (D)
410 Quantitative analysis of control and patient fibroblast mtDNA copy number via quantitative PCR relative
411 to 18S rDNA, analyzed from 2 biological replicates indicated by red and blue colors, with 3 technical
412 replicates each, bar graphs indicate mean +/- SD. (E) Agarose gel image of long-range PCR products from
413 the amplification full-length mtDNA in control and patient cells shows no mtDNA deletions; ladder

414 shown on the left with indicated sizes. For all graphs, p-values were determined by unpaired t-test (*
415 indicates $p \leq 0.05$, ** $p \leq 0.01$, *** $p \leq 0.001$, ***$p \leq 0.0001$).

416

417 **Figure 4- Reduced size and numbers of mitochondrial-ER contact site in patient fibroblasts.**
418 Representative confocal microscopy images for control (A) and patient (B) fibroblasts showing
419 mitochondria (anti-TOMM20; teal), ER (anti-calnexin; magenta), and MERCs (PLA probes; yellow)
420 channels alone and merged. The top panel shows an entire cell, while the bottom panel shows the
421 zoomed-in region indicated by the boxed region above. Quantitative analyses of the average MERC
422 puncta size (C) and number(D) per cell as analyzed from 2 biological replicates with 15 cells for each
423 condition. Violin plots show median and interquartile range. Bar graphs indicate mean and SD with
424 biological replicates indicated by red and blue colors. For all graphs, p-values were determined by
425 unpaired t-test (* indicates $p \leq 0.05$, ** $p \leq 0.01$, *** $p \leq 0.001$, ***$p \leq 0.0001$).

426

427 **Figure 5: Increased size and numbers of lipid droplets patient fibroblasts.** (A) Representative confocal
428 images from control (top) and patient (bottom) fibroblasts stained for lipid droplets (anti-PLIN1; teal)
429 and mitochondria (anti-TOMM20; magenta), far right panel shows zoom inset of white box region.
430 Quantification of mean lipid droplet number (B) and size (C) per cell in control and patient fibroblasts
431 analyzed from 3 biological replicates indicated by red, yellow, blue colors, with 10 cells for each sample.
432 Bar graphs show mean +/- SD. Violin plots indicate media and quartile ranges, while lines show median
433 and +/- SD. For all graphs, p-values were determined by unpaired t-test (* indicates $p \leq 0.05$, ** $p \leq 0.01$,
434 *** $p \leq 0.001$, ***$p \leq 0.0001$).

435

436 **Figure 6: Reduced Complex-I protein level and activity in patient fibroblasts.** (A) Representative
437 western blot images from control and MFN2 R334K patient fibroblasts, showing protein levels of MFN2
438 and the indicate oxidative phosphorylation complex proteins, as well as a beta-Actin loading control and
439 HSP60 as a mitochondrial loading control. (B) Quantification of MFN2 protein levels in control fibroblasts
440 and patient fibroblasts relative to Beta-Actin; analyzed from two biological replicates (red and blue on
441 graph) with three technical replicates for each; bar graphs indicate mean +/- SD. (C) Quantification of
442 mitochondrial oxidative phosphorylation complex proteins (C-I: NDUFB8, C-II: SDHB, C-III: UQCRC2, C-IV:
443 COX II , C-V: ATP5A) from western blot analyses in control and patient fibroblasts normalized to cellular

444 beta-actin levels, analyzed from two biological replicates (red and blue on graph) with three technical
445 replicates for each, lines indicate mean +/- SD. (D) Images of Complex I activity from control and patient
446 fibroblasts, obtained using a complex-I dipstick assay, with quantification of relative complex-I activity
447 (E), analyzed from two biological replicates (blue and red on graph) with three technical replicates, bar
448 graphs indicate mean +/- SD. For all graphs, p-values were determined by unpaired t-test (* indicates $p \leq$
449 0.05, ** $p \leq 0.01$, *** $p \leq 0.001$, ***$p \leq 0.0001$).

450 **References:**

451 1. Polke JM, Laurá M, Pareyson D, et al. Recessive axonal Charcot-Marie-Tooth disease due to
452 compound heterozygous mitofusin 2 mutations. *Neurology*. 2011;77(2):168-173.
453 doi:10.1212/WNL.0b013e3182242d4d

454 2. Hikiami R, Yamashita H, Koita N, et al. Charcot-Marie-Tooth disease type 2A with an autosomal-
455 recessive inheritance: the first report of an adult-onset disease. *J Hum Genet*. 2018;63(1):89-92.
456 doi:10.1038/s10038-017-0353-3

457 3. Chen H, Detmer SA, Ewald AJ, Griffin EE, Fraser SE, Chan DC. Mitofusins Mfn1 and Mfn2 coordinately
458 regulate mitochondrial fusion and are essential for embryonic development. *J Cell Biol*.
459 2003;160(2):189-200. doi:10.1083/jcb.200211046

460 4. Kimura Y, Nishikawa A, Hashiguchi A, et al. An MFN2-related Charcot-Marie-Tooth Disease Patient
461 with Optic Nerve Atrophy, Neurogenic Bladder Dysfunction, and Diaphragmatic Weakness. *Intern*
462 *Med*. 2022;61(11):1743-1747. doi:10.2169/internalmedicine.6487-20

463 5. Sawyer SL, Cheuk-Him Ng A, Innes AM, et al. Homozygous mutations in MFN2 cause multiple
464 symmetric lipomatosis associated with neuropathy. *Hum Mol Genet*. 2015;24(18):5109-5114.
465 doi:10.1093/hmg/ddv229

466 6. Sharma G, Zaman M, Sabouny R, et al. Characterization of a novel variant in the HR1 domain of MFN2
467 in a patient with ataxia, optic atrophy and sensorineural hearing loss. *F1000Res*. 2022;10:606.
468 doi:10.12688/f1000research.53230.2

469 7. Bombelli F, Stojkovic T, Dubourg O, et al. Charcot-Marie-Tooth Disease Type 2A: From Typical to Rare
470 Phenotypic and Genotypic Features. *JAMA Neurology*. 2014;71(8):1036-1042.
471 doi:10.1001/jamaneurol.2014.629

472 8. Chung KW. Early onset severe and late-onset mild Charcot-Marie-Tooth disease with mitofusin 2
473 (MFN2) mutations. *Brain*. 2006;129(8):2103-2118. doi:10.1093/brain/awl174

474 9. Feely SME, Laura M, Siskind CE, et al. MFN2 mutations cause severe phenotypes in most patients
475 with CMT2A. *Neurology*. 2011;76(20):1690-1696. doi:10.1212/WNL.0b013e31821a441e

476 10. Chevrollier A, Bonnard AA, Ruaud L, et al. Homozygous MFN2 variants causing severe antenatal
477 encephalopathy with clumped mitochondria. *Brain*. 2024;147(1):91-99. doi:10.1093/brain/awad347

478 11. de Brito OM, Scorrano L. Mitofusin 2 tethers endoplasmic reticulum to mitochondria. *Nature*.
479 2008;456(7222):605-610. doi:10.1038/nature07534

480 12. Boutant M, Kulkarni SS, Joffraud M, et al. Mfn2 is critical for brown adipose tissue thermogenic
481 function. *EMBO J*. 2017;36(11):1543-1558. doi:10.15252/embj.201694914

482 13. Misko A, Jiang S, Wegorzewska I, Milbrandt J, Baloh RH. Mitofusin 2 is necessary for transport of
483 axonal mitochondria and interacts with the Miro/Milton complex. *J Neurosci*. 2010;30(12):4232-4240.
484 doi:10.1523/JNEUROSCI.6248-09.2010

485 14. McLelland GL, Goiran T, Yi W, et al. Mfn2 ubiquitination by PINK1/parkin gates the p97-
486 dependent release of ER from mitochondria to drive mitophagy. Dikic I, ed. *eLife*. 2018;7:e32866.
487 doi:10.7554/eLife.32866

488 15. Sidarala V, Zhu J, Levi-D'Ancona E, et al. Mitofusin 1 and 2 regulation of mitochondrial DNA
489 content is a critical determinant of glucose homeostasis. *Nat Commun*. 2022;13(1):2340.
490 doi:10.1038/s41467-022-29945-7

491 16. Ainbinder A, Boncompagni S, Protasi F, Dirksen RT. Role of Mitofusin-2 in mitochondrial
492 localization and calcium uptake in skeletal muscle. *Cell Calcium*. 2015;57(1):14-24.
493 doi:10.1016/j.ceca.2014.11.002

494 17. Zaman M, Shutt TE. The Role of Impaired Mitochondrial Dynamics in MFN2-Mediated Pathology.
495 *Front Cell Dev Biol*. 2022;10:858286. doi:10.3389/fcell.2022.858286

496 18. Di Tommaso P, Moretti S, Xenarios I, et al. T-Coffee: a web server for the multiple sequence
497 alignment of protein and RNA sequences using structural information and homology extension.
498 *Nucleic Acids Res*. 2011;39(Web Server issue):W13-17. doi:10.1093/nar/gkr245

499 19. UniProt Consortium. UniProt: the Universal Protein Knowledgebase in 2023. *Nucleic Acids Res*.
500 2023;51(D1):D523-D531. doi:10.1093/nar/gkac1052

501 20. Sabouny R, Wong R, Lee-Glover L, et al. Characterization of the C584R variant in the mtDNA
502 depletion syndrome gene FBXL4, reveals a novel role for FBXL4 as a regulator of mitochondrial fusion.
503 *Biochim Biophys Acta Mol Basis Dis*. 2019;1865(11):165536. doi:10.1016/j.bbadis.2019.165536

504 21. Valente AJ, Maddalena LA, Robb EL, Moradi F, Stuart JA. A simple ImageJ macro tool for
505 analyzing mitochondrial network morphology in mammalian cell culture. *Acta Histochem*.
506 2017;119(3):315-326. doi:10.1016/j.acthis.2017.03.001

507 22. Eaton JS, Lin ZP, Sartorelli AC, Bonawitz ND, Shadel GS. Ataxia-telangiectasia mutated kinase
508 regulates ribonucleotide reductase and mitochondrial homeostasis. *J Clin Invest*. 2007;117(9):2723-
509 2734. doi:10.1172/JCI31604

510 23. Tan CA, Rabideau M, Blevins A, et al. Autosomal recessive MFN2-related Charcot-Marie-Tooth
511 disease with diaphragmatic weakness: Case report and literature review. *Am J Med Genet A*.
512 2016;170(6):1580-1584. doi:10.1002/ajmg.a.37611

513 24. Nicholson GA, Magdelaine C, Zhu D, et al. Severe early-onset axonal neuropathy with
514 homozygous and compound heterozygous MFN2 mutations. *Neurology*. 2008;70(19):1678-1681.
515 doi:10.1212/01.wnl.0000311275.89032.22

516 25. Formosa LE, Mimaki M, Frazier AE, et al. Characterization of mitochondrial FOXRED1 in the
517 assembly of respiratory chain complex I. *Hum Mol Genet*. 2015;24(10):2952-2965.
518 doi:10.1093/hmg/ddv058

519 26. Apatean D, Rakic B, Brunel-Guitton C, et al. Congenital lactic acidosis, cerebral cysts and
520 pulmonary hypertension in an infant with FOXRED1 related complex I deficiency. *Mol Genet Metab*
521 *Rep*. 2019;18:32-38. doi:10.1016/j.ymgmr.2018.12.006

522 27. Lemire BD. Evolution of FOXRED1, an FAD-dependent oxidoreductase necessary for
523 NADH:ubiquinone oxidoreductase (Complex I) assembly. *Biochim Biophys Acta*. 2015;1847(4-5):451-
524 457. doi:10.1016/j.bbabio.2015.01.014

525 28. Fassone E, Duncan AJ, Taanman JW, et al. FOXRED1, encoding an FAD-dependent
526 oxidoreductase complex-I-specific molecular chaperone, is mutated in infantile-onset mitochondrial
527 encephalopathy. *Hum Mol Genet*. 2010;19(24):4837-4847. doi:10.1093/hmg/ddq414

528 29. Silva Ramos E, Motori E, Brüser C, et al. Mitochondrial fusion is required for regulation of
529 mitochondrial DNA replication. *PLoS Genet*. 2019;15(6):e1008085. doi:10.1371/journal.pgen.1008085

530 30. Renaldo F, Amati-Bonneau P, Slama A, et al. MFN2, a new gene responsible for mitochondrial
531 DNA depletion. *Brain*. 2012;135(Pt 8):e223, 1-4; author reply e224, 1-3. doi:10.1093/brain/aws111

532 31. Larrea D, Pera M, Gonnelli A, et al. MFN2 mutations in Charcot-Marie-Tooth disease alter
533 mitochondria-associated ER membrane function but do not impair bioenergetics. *Hum Mol Genet*.
534 2019;28(11):1782-1800. doi:10.1093/hmg/ddz008

535 32. Benhammouda S, Vishwakarma A, Gatti P, Germain M. Mitochondria Endoplasmic Reticulum
536 Contact Sites (MERCs): Proximity Ligation Assay as a Tool to Study Organelle Interaction. *Front Cell*
537 *Dev Biol*. 2021;9:789959. doi:10.3389/fcell.2021.789959

538 33. Züchner S, De Jonghe P, Jordanova A, et al. Axonal neuropathy with optic atrophy is caused by
539 mutations in mitofusin 2. *Ann Neurol*. 2006;59(2):276-281. doi:10.1002/ana.20797

540 34. Rouzier C, Bannwarth S, Chaussenot A, et al. The MFN2 gene is responsible for mitochondrial
541 DNA instability and optic atrophy "plus" phenotype. *Brain*. 2012;135(Pt 1):23-34.
542 doi:10.1093/brain/awr323

543 35. Pellino G, Faggioli R, Galuppi A, et al. Mitofusin 2: The missing link between mtDNA maintenance
544 defects and neurotransmitter disorders. *Mitochondrion*. 2021;61:159-164.
545 doi:10.1016/j.mito.2021.09.011

546 36. Madrid R, Guariglia SR, Haworth A, Korosh W, Gavin M, Lyon GJ. Early-onset cerebellar ataxia in
547 a patient with CMT2A2. *Cold Spring Harb Mol Case Stud*. 2020;6(3):a005108.
548 doi:10.1101/mcs.a005108

549 37. Eschenbacher WH, Song M, Chen Y, et al. Two rare human mitofusin 2 mutations alter
550 mitochondrial dynamics and induce retinal and cardiac pathology in Drosophila. *PLoS One*.
551 2012;7(9):e44296. doi:10.1371/journal.pone.0044296

552 38. Vielhaber S, Debska-Vielhaber G, Peeva V, et al. Mitofusin 2 mutations affect mitochondrial
553 function by mitochondrial DNA depletion. *Acta Neuropathol*. 2013;125(2):245-256.
554 doi:10.1007/s00401-012-1036-y

555 39. Loiseau D, Chevrollier A, Verny C, et al. Mitochondrial coupling defect in Charcot-Marie-Tooth
556 type 2A disease. *Ann Neurol*. 2007;61(4):315-323. doi:10.1002/ana.21086

557 40. Luo N, Yue F, Jia Z, et al. Reduced electron transport chain complex I protein abundance and
558 function in Mfn2-deficient myogenic progenitors lead to oxidative stress and mitochondria swelling.
559 *FASEB J*. 2021;35(4):e21426. doi:10.1096/fj.202002464R

560 41. Pagliarini DJ, Calvo SE, Chang B, et al. A mitochondrial protein compendium elucidates complex I
561 disease biology. *Cell*. 2008;134(1):112-123. doi:10.1016/j.cell.2008.06.016

562 42. Hu C, Xu Q, Shen J, Wang Y. Clinical and Genetic Characteristics of Mitochondrial
563 Encephalopathy Due to FOXRED1 Mutations: Two Chinese Case Reports and a Review of the
564 Literature. *Front Neurol*. 2021;12:633397. doi:10.3389/fneur.2021.633397

565 43. Calvo SE, Tucker EJ, Compton AG, et al. High-throughput, pooled sequencing identifies
566 mutations in NUBPL and FOXRED1 in human complex I deficiency. *Nat Genet*. 2010;42(10):851-858.
567 doi:10.1038/ng.659

568 44. Zurita Rendón O, Antonicka H, Horvath R, Shoubridge EA. A Mutation in the Flavin Adenine
569 Dinucleotide-Dependent Oxidoreductase FOXRED1 Results in Cell-Type-Specific Assembly Defects in
570 Oxidative Phosphorylation Complexes I and II. *Mol Cell Biol*. 2016;36(16):2132-2140.
571 doi:10.1128/MCB.00066-16

572 45. Haack TB, Madignier F, Herzer M, et al. Mutation screening of 75 candidate genes in 152
573 complex I deficiency cases identifies pathogenic variants in 16 genes including NDUFB9. *J Med Genet*.
574 2012;49(2):83-89. doi:10.1136/jmedgenet-2011-100577

575 46. Marra F, Lunetti P, Curcio R, et al. An Overview of Mitochondrial Protein Defects in
576 Neuromuscular Diseases. *Biomolecules*. 2021;11(11):1633. doi:10.3390/biom11111633

577 47. Chung CCY, Leung GKC, Mak CCY, et al. Rapid whole-exome sequencing facilitates precision
578 medicine in paediatric rare disease patients and reduces healthcare costs. *Lancet Reg Health West*
579 *Pac*. 2020;1:100001. doi:10.1016/j.lanwpc.2020.100001

580 48. McDermott H, Sherlaw-Sturrock C, Baptista J, Hartles-Spencer L, Naik S. Rapid exome
581 sequencing in critically ill children impacts acute and long-term management of patients and their

582 families: A retrospective regional evaluation. *Eur J Med Genet*. 2022;65(9):104571.
583 doi:10.1016/j.ejmg.2022.104571

584 49. Freed AS, Clowes Candadai SV, Sikes MC, et al. The Impact of Rapid Exome Sequencing on
585 Medical Management of Critically Ill Children. *J Pediatr*. 2020;226:202-212.e1.
586 doi:10.1016/j.jpeds.2020.06.020

587

(A)

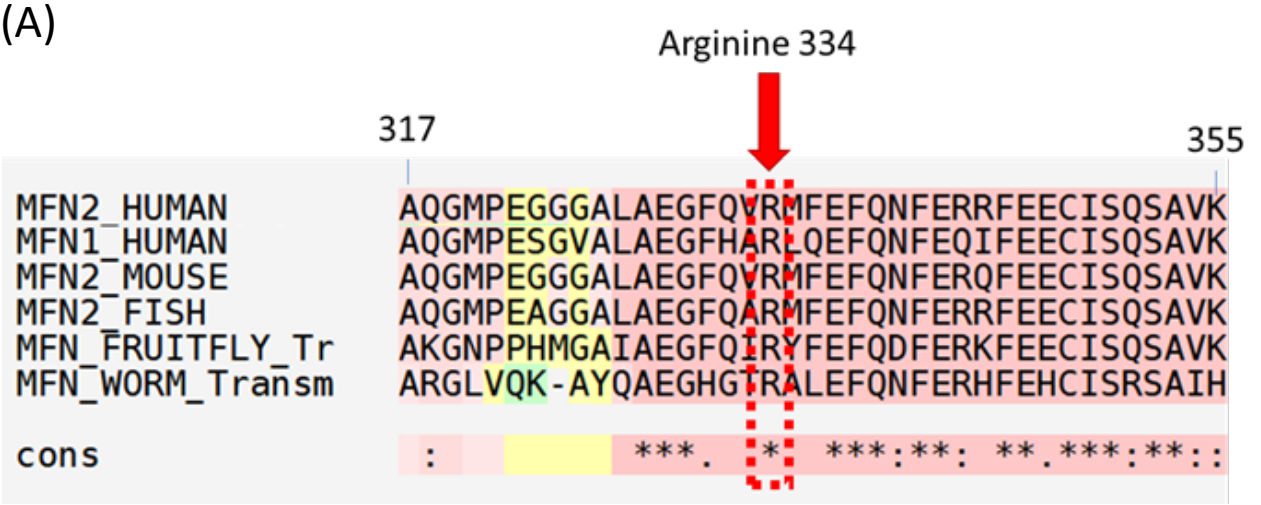
Arginine 334
317
355
MFN2_HUMAN AQGMPEGGGALAEGFQVRMFEFQNFERRFEECISQSAVK
MFN1_HUMAN AQGMPESGVALAEGFHARLQEFQNFEQIFEECISQSAVK
MFN2_MOUSE AQGMPEGGGALAEGFQVRMFEFQNFERQFEECISQSAVK
MFN2_FISH AQGMPEAGGALAEGFQARMFEFQNFERRFEECISQSAVK
MFN_FRUITFLY_Tr AKGNPPHMGAIAEGFQIRYFEFQDFERKFEECISQSAVK
MFN_WORM_Transm ARGLVQK-AYQAEGHGTRALEFQNFERHFEHCISRSAIH
cons : ***. * ***:**: **.***:**::

(B)

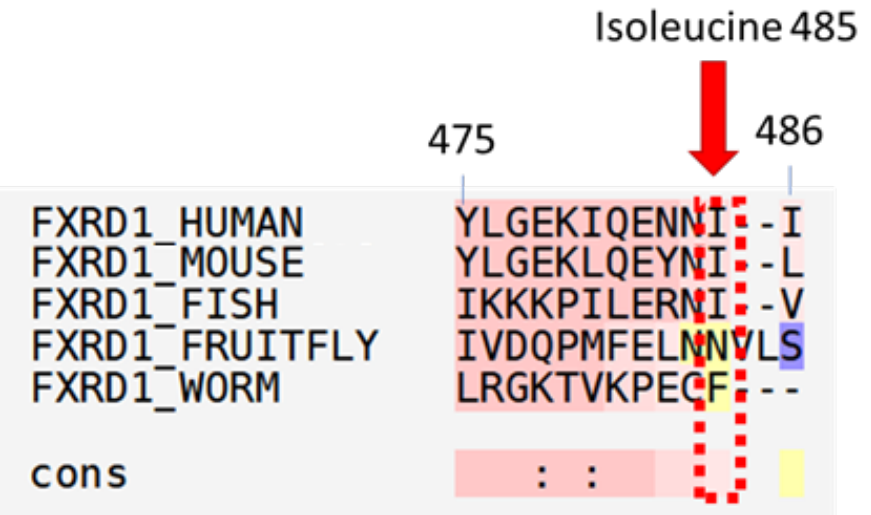
Isoleucine 485
475
486
FXRD1_HUMAN YLGEKIQENNI--I
FXRD1_MOUSE YLGEKLQEYNI--L
FXRD1_FISH IKKKPILERNI--V
FXRD1_FRUITFLY IVDQPMFELNNVLS
FXRD1_WORM LRGKTVKPECF---
cons : :

Figure 1

A.

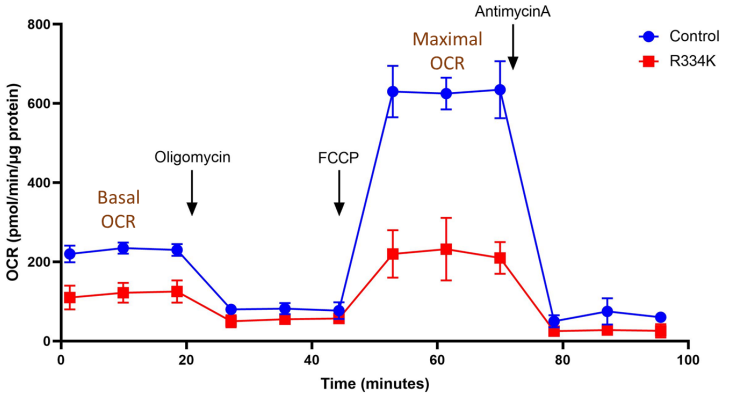

B.

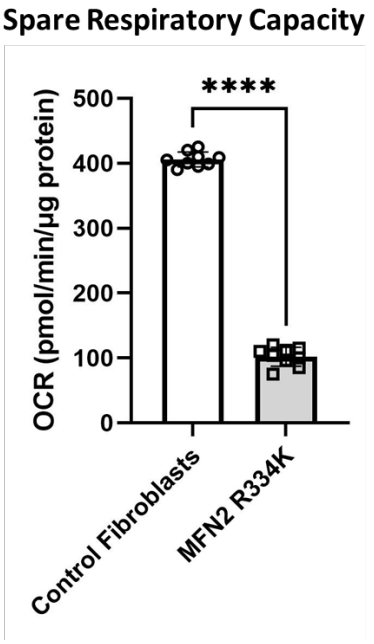

C.

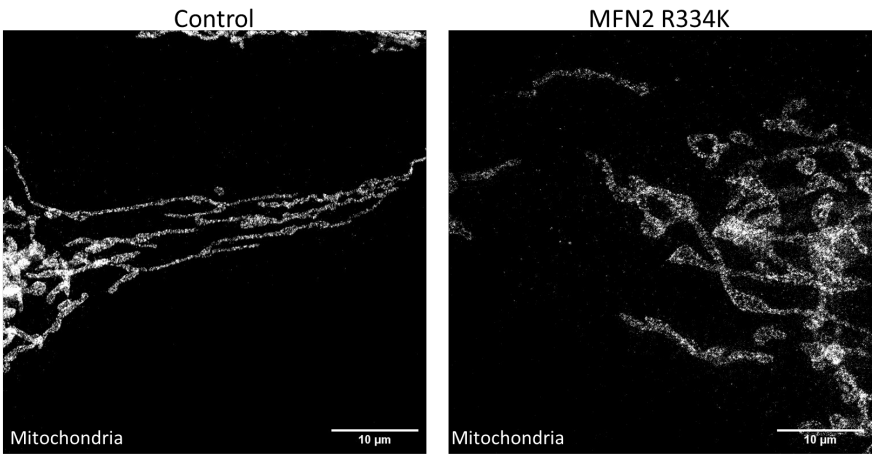

D.

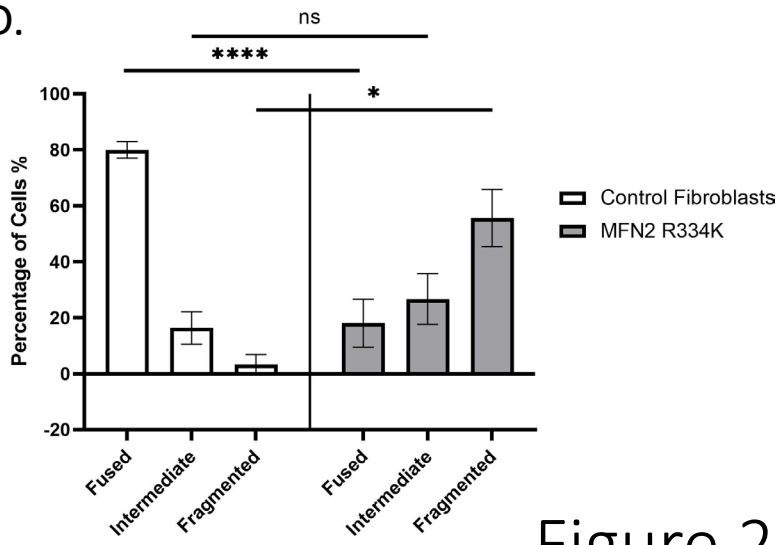

E.

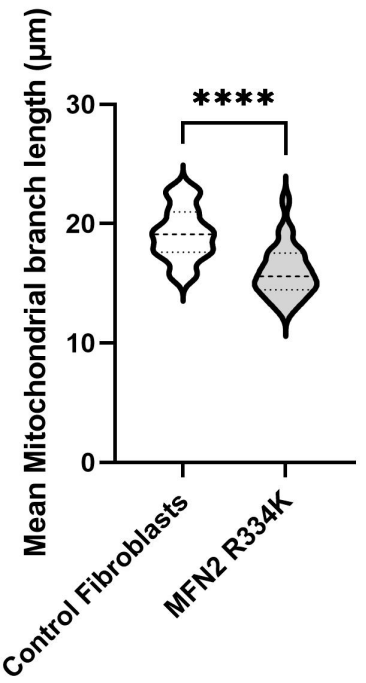

Figure 2

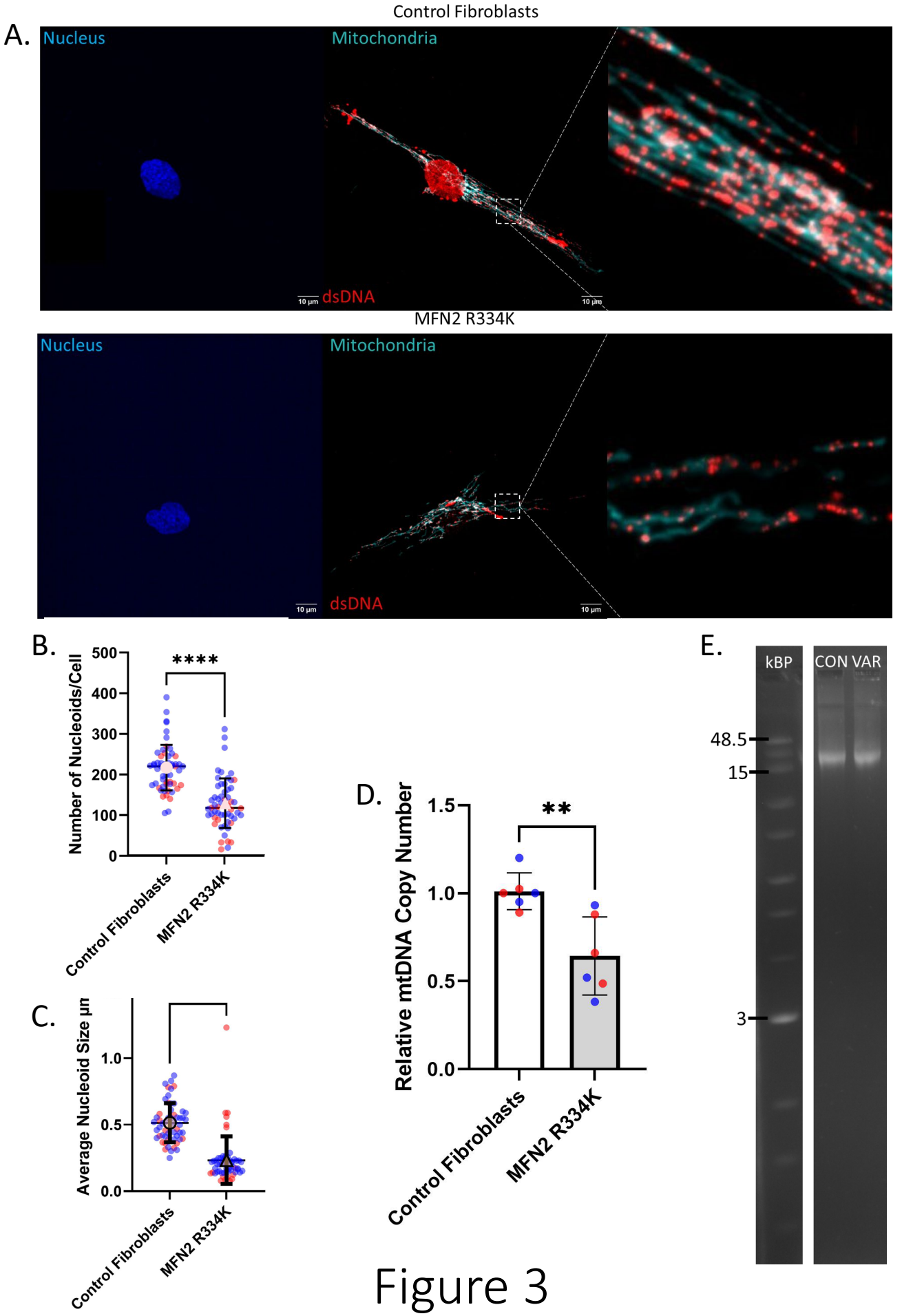
A.
Control Fibroblasts
Nucleus
Mitochondria
dsDNA
10 µm
MFN2 R334K
Nucleus
Mitochondria
dsDNA
10 µm
B.
Number of Nucleoids/Cell
500
400
300
200
100
0
****
Control Fibroblasts
MFN2 R334K
C.
Average Nucleoid Size µm
1.0
0.5
0.0
Control Fibroblasts
MFN2 R334K
D.
Relative mtDNA Copy Number
1.5
1.0
0.5
0.0
**
Control Fibroblasts
MFN2 R334K
E.
kBP
CON VAR
48.5
15
3

Figure 3

A.

Control

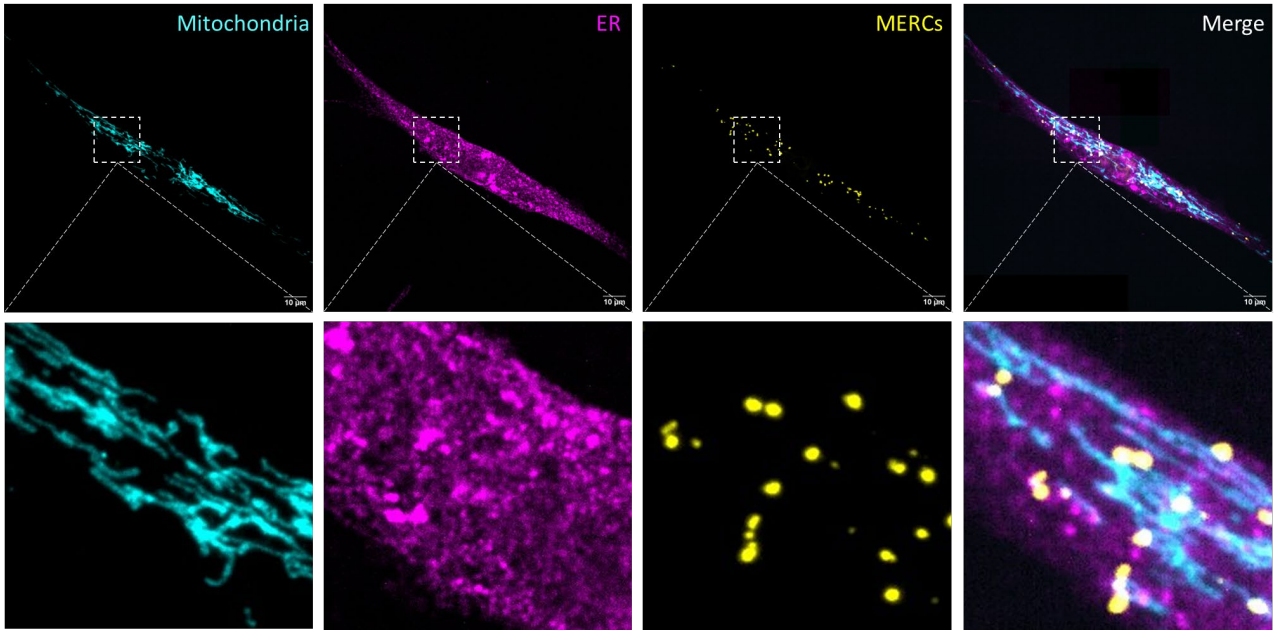

B.

MFN2 R334K

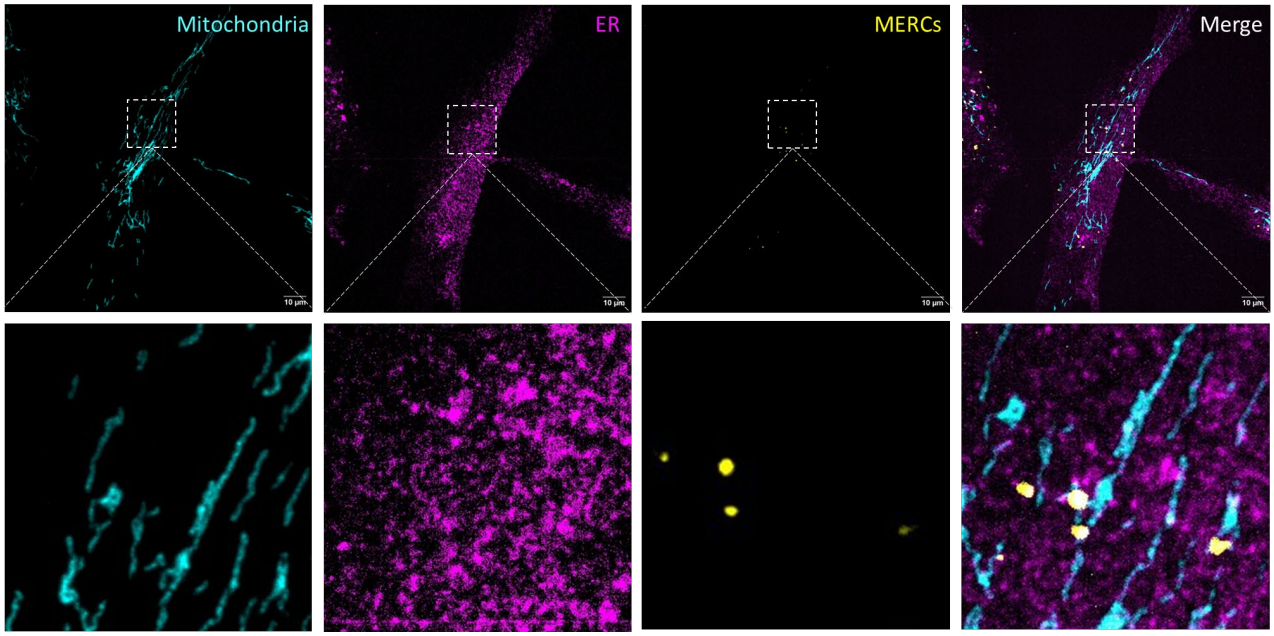

C.

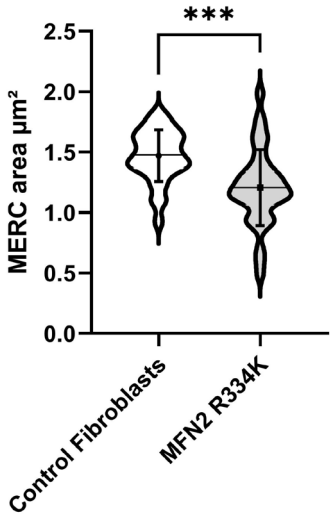

D.

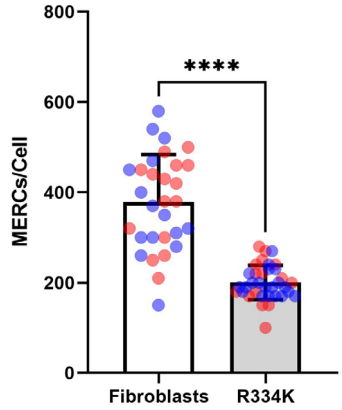

Figure 4

A.

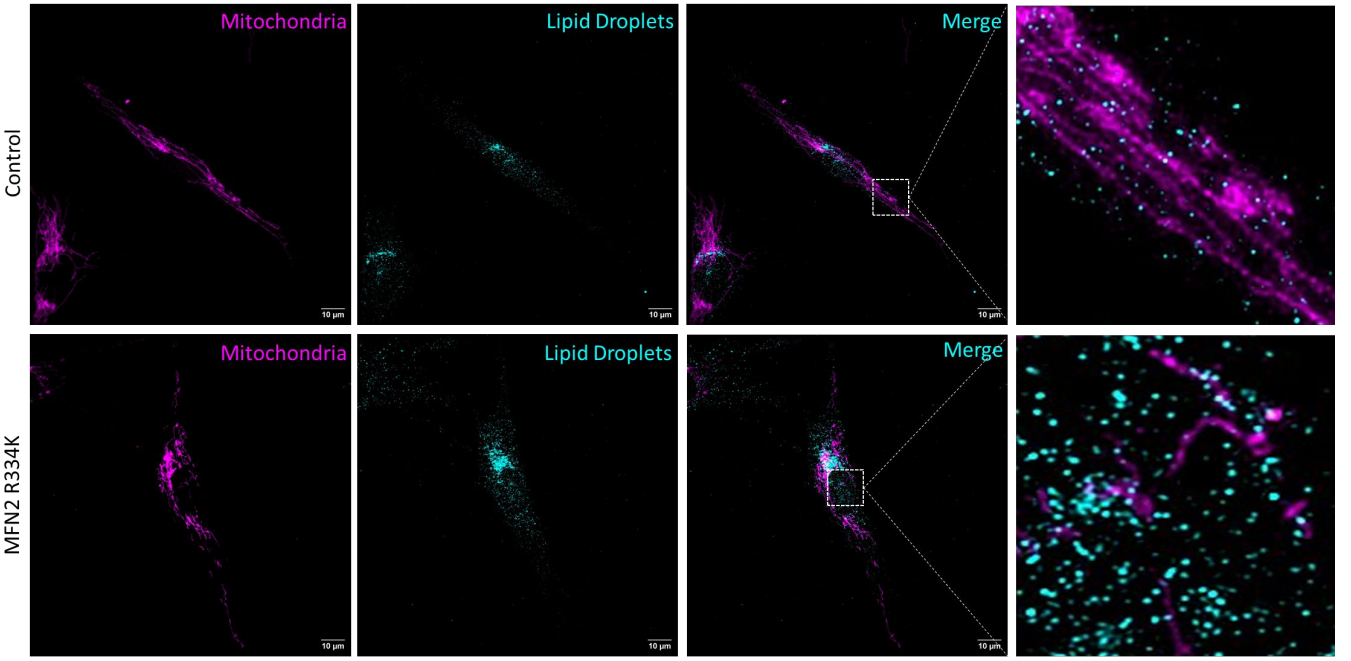
Mitochondria
Lipid Droplets
Merge
Control
MFN2 R334K
10 µm

B.

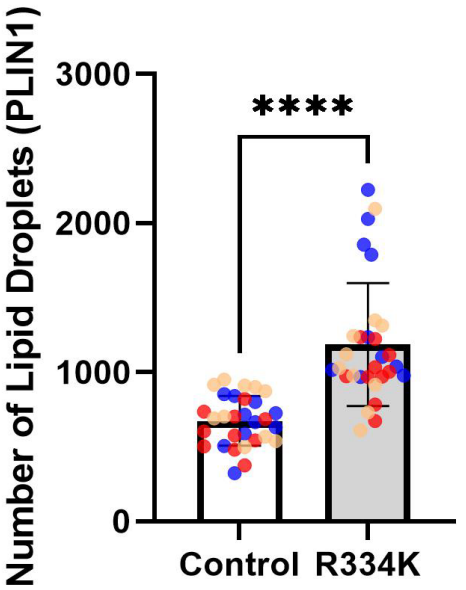
Number of Lipid Droplets (PLIN1)
3000
2000
1000
0
****
Control
R334K

C.

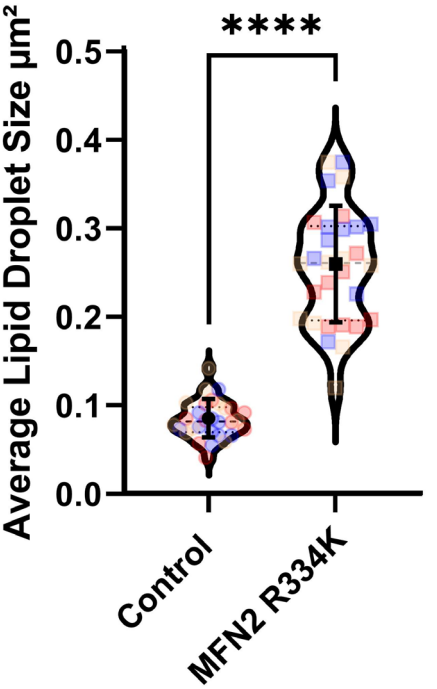
Average Lipid Droplet Size µm²
0.5
0.4
0.3
0.2
0.1
0.0
****
Control
MFN2 R334K

Figure 5

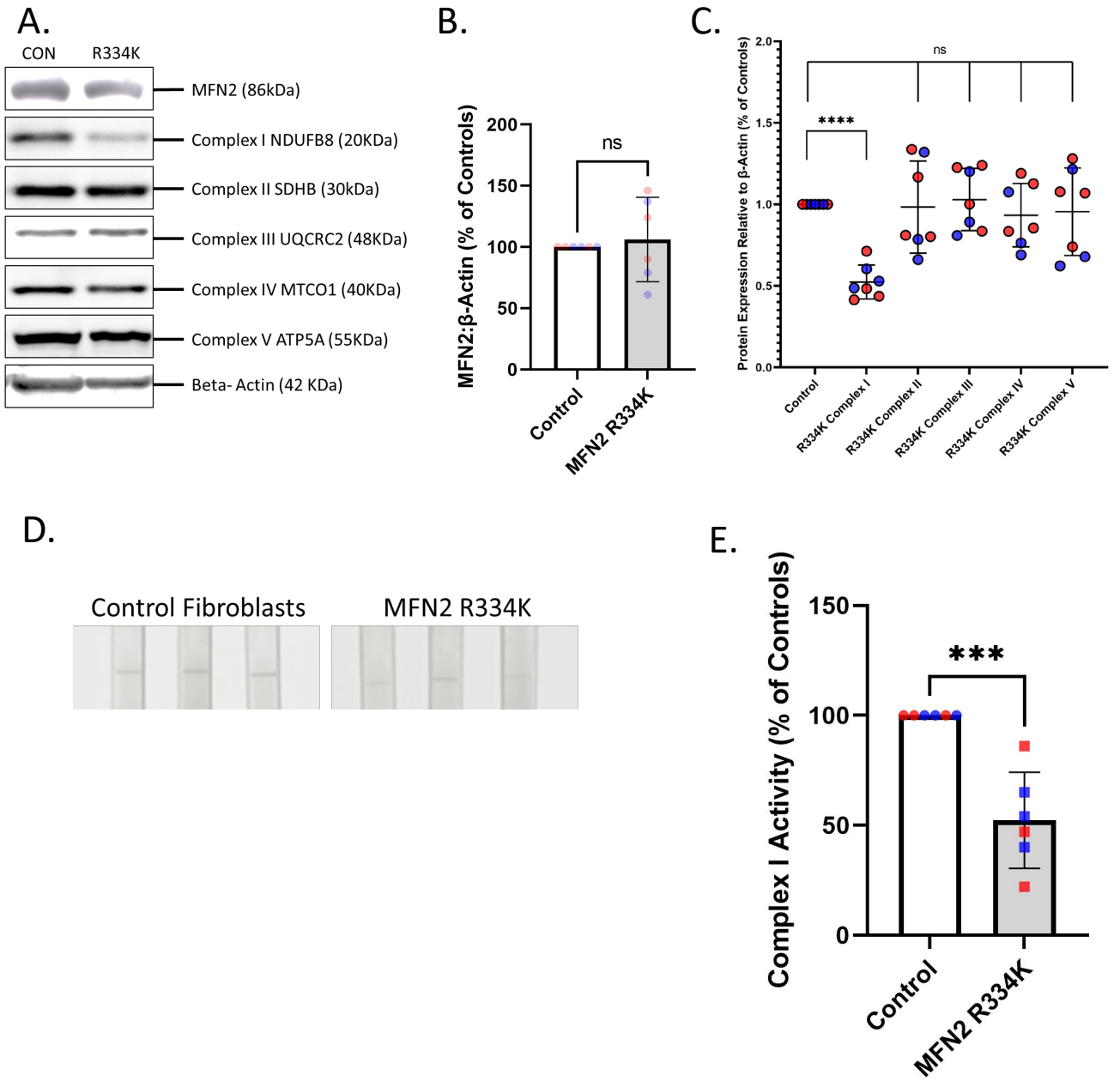
A.
CON
R334K
MFN2 (86kDa)
Complex I NDUFB8 (20KDa)
Complex II SDHB (30kDa)
Complex III UQCRC2 (48KDa)
Complex IV MTCO1 (40KDa)
Complex V ATP5A (55KDa)
Beta- Actin (42 KDa)
B.
MFN2:β-Actin (% of Controls)
200
150
100
50
0
ns
Control
MFN2 R334K
C.
Protein Expression Relative to β-Actin (% of Controls)
2.0
1.5
1.0
0.5
0.0
ns
****
Control
R334K Complex I
R334K Complex II
R334K Complex III
R334K Complex IV
R334K Complex V
D.
Control Fibroblasts
MFN2 R334K
E.
Complex I Activity (% of Controls)
150
100
50
0
***
Control
MFN2 R334K

Figure 6